Nonlinear Diffussion-Advection-Reaction Phenomena Involved in the Pumping of Oil from Open Sea: Modeling and Numerical Simulation.

Benjamin Ivorra[1], Susana Gomez[2]
Roland Glowinski[3] Angel Manuel Ramos[1]

[1] Departamento de Matemática Aplicada,
Universidad Complutense de Madrid,
Plaza de Ciencias 3, 28040, Madrid, Spain

[2] Instituto de Matematicas Aplicadas y Sistemas,
Universidad Nacional A. de Mexico, Mexico

[3] Department of Mathematics, University of Houston,
651 P. G. Hoffman Hall, Houston, TX 77204-3008, USA

March 20, 2015

Abstract

The main goal of this article is to improve upon a previous model used to simulate the evolution of oil spots in the open sea and the effect of a skimmer ship pumping oil out of the spots. The concentration of the pollutant is subject to the effects of wind and sea currents, diffusion, and the pumping action of a skimmer (i.e., cleaning) ship that follows a pre-assigned trajectory. This implies that the mathematical model is of the advection-reaction-diffusion type. A drawback of our previous model was that diffusion was propagating with infinite velocity; in this article, we use an improved modeling relying on a nonlinear diffusion term, implying that diffusion propagates with finite velocity. To reduce numerical diffusion when approximating the advection part of the model, we consider second order discretization schemes with nonlinear flux limiters. We consider also absorbing boundary conditions to insure accurate results near the boundary. Finally, to reduce CPU time we use an operator-splitting scheme for the time discretization. The novel approach we advocate in this article is validated by

comparing our numerical results with real life measurements from the Prestige oil spill which took place in Spain in 2002.

Keywords: *Advection-reaction-diffusion equations; Sea pollution; Skimmer ship; nonlinear diffusion; second order advection; flux-limiters; operator-splitting.*

1 Introduction

Oil spill contamination in open sea has been at the origin of some of the worst environmental disasters in history (see [24, 22, 33]). The ecological and economical impact of such hazards are generally important and should be controlled as quickly as possible. For instance in 1989, the Exxon Valdez tanker sank near Alaska, spilling more than 10 million gallons of crude oil [26]. It was estimated that more than 50% of the sea birds and otters of the area were killed. The cost of depolluting the contaminated zone has been estimated to US$ 287 million.

One of the major cleaning techniques [18, 28] for these hazards is the use of skimmer ships [5]. Those ships use various pumps distributed along its waterline to suck the oil from the surface of the water directly into storage units. Those vessels move inside the oil spots to clean them as quickly as possible.

In previous works, we have been interested in improving this process. To do so, we first introduce a numerical model to simulate the effect the skimmer ship on the evolution of the oil spill [2]. This model, based on a first order finite volume approximation of an advection-diffusion-reaction equation [11, 15], took into consideration: the motion of oil spots resulting from the combined effects of diffusion and of transport by wind and sea currents, and also the physical phenomena associated with the action of the pumping ship, assuming that it follows a pre-assigned trajectory. In a second article [12], we have designed the trajectory of a skimmer ship in order to maximize the amount of recovered oil. Actually, the model and methodology we used in these previous studies require various modifications and improvements, such as:

- Use a diffusion model leading to diffusion propagating at finite speed.
- Reduce the numerical diffusion resulting from the discretization of the advection term in the model.
- Use boundary conditions with better absorbing properties.

- Reduce the computational complexity.

These various issues will be addressed in this article. We introduce in particular a nonlinear diffusion term to obtain a diffusion propagating at finite speed. Next, we discuss an absorbing boundary condition, to handle those situations when the oil is exiting the computational domain. Then, to reduce numerical diffusion, we use second order numerical schemes for the discretization of the advection terms of the model. Finally, we discuss the use of splitting and un-split schemes and their impact on the computational complexity. To validate this new methodology, we compare the numerical results its produces to measurements from the real Prestige oil spill hazard, which occurred in Spain in 2002 [19].

The content of this article is as follows: In Section 2, we present the old and new mathematical **models we** consider to simulate the motion of the oil spots and the action of the pumping ship. In Section 3, we discuss the numerical methods to be used for these simulations. Finally, in Section 4, we describe the numerical experiments and discuss their results, including comparisons with measurements from a real life disaster, the 2002 Prestige oil spill.

2 Mathematical models

2.1 Generalities

We consider a spatial domain $\Omega = (x_{\min}, x_{\max}) \times (y_{\min}, y_{\max}) \subset \mathbb{R}^2$, large enough to ensure that the pollutant will stay in Ω during the corresponding fixed time interval $(0, T)$.

We assume that the density of the pollutant is smaller than the one of the sea water (so that it remains at the top); we assume also that the layer-thickness of the pollutant is a known constant that we will denote by h [23]. We denote by $c(x, t)$ the pollutant superficial concentration, measured as the volume of pollutant per surface area at $\{x, t\} \in \Omega \times (0, T)$. We assume that the evolution of c is governed by five main effects, namely:

- The *diffusion* of the pollutant.
- The *wind* induced transport.
- The *sea current* induced transport.
- The transport and *sink* resulting from the *pumping*

Moreover, we assume that the pumping ship follows a trajectory $\gamma \in C^0([0,T],\mathbb{R}^2)$, such that $\gamma(t) \in \Omega, \forall t \in [0,T]$.

From a practical point of view, a skimmer ship is composed of multiple pumps, cleaning the water along the vessel waterline. For simplicity (as in the numerical experiments discussed in Section 4), we neglect the length of the ship compared to the size of Ω. We **suppose** also that there is only one pump, which is a circle of radius R_p, pumping the fluid with velocity Q in the radial direction.

2.2 The previous model

In [2], we considered a simple model, assuming linear diffusion and homogeneous boundary conditions. We considered, more precisely:

$$\begin{cases} \dfrac{\partial c}{\partial t} - \nabla \cdot \mathbf{d}\nabla c + \nabla \cdot c\,\mathbf{w} + \nabla \cdot c\,\mathbf{s} \\ \qquad\qquad +\nabla \cdot c\,\mathbf{p} = -\dfrac{2Q}{R_p}\, c\ \chi_{B(\gamma(t),R_p)}, & \text{in } \Omega \times (0,T), \\ c = 0, & \text{on } \partial\Omega \times (0,T), \\ c(0) = c_0, \end{cases} \tag{1}$$

where:

- $c(t)$ denotes the function $x \to c(x,t)$.
- $B(\gamma(t),R_p)$ is the ball of center $\gamma(t)$ and radius R_p.
- $\mathbf{p}(\xi,t) = \begin{cases} QR_p \dfrac{\overrightarrow{\gamma(t)\xi}}{(\|\overrightarrow{\gamma(t)\xi}\|_2)^2}, & \text{if } \xi \in \Omega\backslash B(\gamma(t),R_p), \\ 0, & \text{if } \xi \in B(\gamma(t),R_p), \end{cases}$ see details in [2].
- $\chi_{B(\gamma(t),R_p)}(\xi) = \begin{cases} 0, & \text{if } \xi \in \Omega\backslash B(\gamma(t),R_p), \\ 1, & \text{if } \xi \in B(\gamma(t),R_p). \end{cases}$
- The function c_0 is the initial superficial concentration; we assume that c_0 has a compact support in Ω.
- $\mathbf{d} = \begin{pmatrix} d_1 & 0 \\ 0 & d_2 \end{pmatrix}$, d_1, d_2 (both >0) being the diffusion coefficients in the west-east and south-north directions.

- **w** is the horizontal components of the wind velocity multiplied by a suitable drag factor.
- **s** is the see current velocity.

2.3 An improved model

Two important drawbacks of the model described in Section 2.2 are: (i) the diffusion propagates at infinite speed, and (ii) **if** discretized using a first order up-winding scheme the advection terms in (1) generate artificial diffusion, implying that a small quantity of oil always gets out of Ω. Moreover, the Dirichlet boundary condition ($c = 0$) makes sense only as long as the pollutant does not reach the boundary of Ω (or if only small quantities reach that boundary).

In this article, we have improved the model developed in [2] (namely the model given by (1)). To do so, we have : (i) replaced the linear diffusion term by a *nonlinear* one, and (ii) replaced the boundary condition $c = 0$ on $\partial\Omega \times (0,T)$ by one with better *absorbing properties*. The new model is given by

$$\begin{cases} \dfrac{\partial c}{\partial t} - \nabla \cdot \dfrac{c^\kappa}{c_{\text{ref}}^\kappa} \mathbf{d} \nabla c + \nabla \cdot c\, \mathbf{w} + \nabla \cdot c\, \mathbf{s} \\ \qquad\qquad + \nabla \cdot c\, \mathbf{p}_{\text{tol}} = -\dfrac{2Q}{R_p}\, c\ \chi_{B(\gamma(t),R_p)}, & \text{in } \Omega \times (0,T), \\ L \dfrac{\partial c}{\partial t} + \Big[-(\mathbf{w} + \mathbf{s} + \mathbf{p}_{\text{tol}})c + \dfrac{c^\kappa}{c_{\text{ref}}^\kappa} \mathbf{d} \nabla c \Big] \cdot \mathbf{n} = 0, & \text{on } \partial\Omega \times (0,T), \\ c(0) = c_0, \end{cases} \tag{2}$$

where:

- $\mathbf{p}_{\text{tol}}(\xi,t) = \max\Big(\dfrac{\|\mathbf{p}(\xi,t)\|_2 - \text{tol}}{Q - \text{tol}}, 0\Big) \cdot \mathbf{p}(\xi,t)$ is a corrected approximation of the velocity pump. This expression means that (i) the effect of the velocity field $\mathbf{p}$ on oil particles is neglected (i.e., $\mathbf{p}_{\text{tol}} = 0$) when $\|\mathbf{p}(\xi,t)\|_2 <$tol, for which the pump velocity is considered negligible regarding the diffusion coefficients; (ii) $\mathbf{p}_{\text{tol}}(\xi,t) = \mathbf{p}(\xi,t)$, when $\|\overrightarrow{\gamma(t)\xi}\|_2 \le R_p$; and (iii) $\mathbf{p}_{\text{tol}}(\xi,t) < \mathbf{p}(\xi,t)$ and $\mathbf{p}_{\text{tol}}(\xi,t)$ is a smooth function, when $\|\overrightarrow{\gamma(t)\xi}\|_2 > R_p$.
- c_{ref} is a reference pollutant concentration (here, $c_{\text{ref}} = 1$), and $\kappa > 0$ (typical values of κ being 1, 2 and 3).

- L is a length, characteristic of the size of the domain Ω, typically the diameter of Ω (that is $L = \sqrt{(x_{\max} - x_{\min})^2 + (y_{\max} - y_{\min})^2}$).

In order to solve (2), we introduce in the next section, a numerical model that includes (a) second order schemes with linear and nonlinear limiters for the discretization of the advective terms, and (b) a time discretization by operator splitting to treat separately the diffusion-sea-wind and the pumping.

3 Numerical methods

Before introducing in Section 3.2 the scheme used to solve numerically (2), we first recall in Section 3.1 the basis of the piecewise linear scheme with limiters in the 1D case with constant velocity [14, 9]. In Section 3.3, we describe the splitting technique used to improve the computational efficiency of the algorithm.

3.1 Review of the piecewise linear schemes and of the limiters

Suppose that we want to approximate the solution of the following 1-D equation

$$\frac{\partial c}{\partial t} + \frac{\partial (vc)}{\partial x} \quad \text{in } \Theta \times (0, T) \tag{3}$$

where c is the concentration, v is the velocity, $\Theta = [\underline{\Theta}, \overline{\Theta}]$, where $\underline{\Theta}$ and $\overline{\Theta}$ belong both to $\mathbb{R}$, and are, respectively, the lower and upper boundaries of the interval Θ. Next, interval Θ is decomposed into I finite volume cells (intervals here), that we denote by $\Theta_i = [x_{i-\frac{1}{2}}, x_{i+\frac{1}{2}}]$. For simplicity of notation, we assume first that $v > 0$ is constant and that the lengths of the intervals Θ_i are all the same, and equal to Δx.

One way to obtain such an approximation is, for instance, to assume that in each finite volume Θ_i, with $i = 1, ..., I$, the concentration c is constant throughout the volume. This simplification allows to generate first order numerical schemes, such as the upwind scheme used in [2]. However, it was observed that this scheme produces a high level of artificial diffusion. To address this issue, it would be better to assume that the concentration within each volume Θ_i is an affine function of the position (see [30]).

In this case, in Θ_i at time t_n the concentration can be linearly approximated by:

$$c(x, t_n) = c_i^n + \sigma_i^n (x - x_i), \text{ for } x \in \Theta_i, \tag{4}$$

where x_i is the center of Θ_i, $c_i^n = c(x_i, t_n)$ and σ_i^n is the slope of the linear approximation. We note that σ_i^n can be defined in several ways. For instance

- $\sigma_i^n = \dfrac{c_{i+1}^n - c_{i-1}^n}{2\Delta x}$, in this case we obtain the Fromm method.
- $\sigma_i^n = \dfrac{c_i^n - c_{i-1}^n}{\Delta x}$, in this case we obtain the Beam-Warming method.
- $\sigma_i^n = \dfrac{c_{i+1}^n - c_i^n}{\Delta x}$, in this case we obtain the Lax-Wendroff method.

For these three cases, c_i^n is equal to the average of $c(x, t_n)$ over Θ_i.

At the boundary $x_{i-\frac{1}{2}}$, the flux $f_{i-\frac{1}{2}}(t)$, with t in the time interval $[t_n, t_{n+1}]$, is:

$$\begin{aligned} f_{i-\frac{1}{2}}(t) &= vc(x_{i-\frac{1}{2}}, t) = vc(x_{i-\frac{1}{2}} - v(t-t_n), t_n) \\ &= vc_{i-1}^n + v\sigma_{i-1}^n \left(\tfrac{1}{2}\Delta x - v(t-t_n)\right). \end{aligned}$$

At the boundary $x_{i+\frac{1}{2}}$, the flux $f_{i+\frac{1}{2}}(t)$, with t in the time interval $[t_n, t_{n+1}]$, is:

$$\begin{aligned} f_{i+\frac{1}{2}}(t) &= vc(x_{i+\frac{1}{2}}, t) = vc(x_{i+\frac{1}{2}} - v(t-t_n), t_n) \\ &= vc_i^n + v\sigma_i^n \left(\tfrac{1}{2}\Delta x - v(t-t_n)\right). \end{aligned}$$

Thus, on the time interval $[t_n, t_{n+1}]$ the variation of concentration over the volume Θ_i is given by

$$\frac{c_i^{n+1} - c_i^n}{\Delta t} = \frac{f_{i-\frac{1}{2}}^{n+\frac{1}{2}} - f_{i+\frac{1}{2}}^{n+\frac{1}{2}}}{\Delta x},$$

where $f_{i\pm\frac{1}{2}}^{n+\frac{1}{2}} = \dfrac{1}{\Delta t}\displaystyle\int_{t_n}^{t_{n+1}} f_{i\pm\frac{1}{2}}(t)\mathrm{dt}$ denotes the flux average during the time interval $[t_n, t_{n+1}]$ which is similar to the flux at $\dfrac{t_{n+1} + t_n}{2}$.

Considering that

$$f_{i-\frac{1}{2}}^{n+\frac{1}{2}} - f_{i+\frac{1}{2}}^{n+\frac{1}{2}} = v(c_{i-1}^n - c_i^n) + \frac{1}{2}v(\sigma_{i-1}^n - \sigma_i^n)(\Delta x - v\Delta t),$$

we obtain the following space-time discretization scheme:

$$c_i^{n+1} = c_i^n + \frac{\Delta t}{\Delta x}\left(v(c_{i-1}^n - c_i^n) + \frac{1}{2}v(\sigma_{i-1}^n - \sigma_i^n)(\Delta x - v\Delta t)\right) \qquad (5)$$

Now, we generalize scheme (5) to the case of non constant velocities $v : \Theta \to \mathbb{R}$.

In this case

$$f_{i-\frac{1}{2}}^{n-\frac{1}{2}} = \frac{1}{2} v_{i-\frac{1}{2}} \left[(1+\beta_{i-\frac{1}{2}}) c_{i-1}^n + (1-\beta_{i-\frac{1}{2}}) c_i^n \right] + \frac{1}{4} |v_{i-\frac{1}{2}}| \left(1 - \left| \frac{v_{i-\frac{1}{2}} \Delta t}{\Delta x} \right| \right) \Delta x \left[(1+\beta_{i-\frac{1}{2}}) \sigma_{i-1}^n + (1-\beta_{i-\frac{1}{2}}) \sigma_i^n \right], \tag{6}$$

and

$$f_{i+\frac{1}{2}}^{n+\frac{1}{2}} = \frac{1}{2} v_{i+\frac{1}{2}} \left[(1+\beta_{i+\frac{1}{2}}) c_i^n + (1-\beta_{i+\frac{1}{2}}) c_{i+1}^n \right] + \frac{1}{4} |v_{i+\frac{1}{2}}| \left(1 - \left| \frac{v_{i+\frac{1}{2}} \Delta t}{\Delta x} \right| \right) \Delta x \left[(1+\beta_{i+\frac{1}{2}}) \sigma_i^n + (1-\beta_{i+\frac{1}{2}}) \sigma_{i+1}^n \right], \tag{7}$$

where $\beta_{i\pm\frac{1}{2}} = 1$ if $v_{i\pm\frac{1}{2}} \geq 0$ or $= -1$ if $v_{i\pm\frac{1}{2}} < 0$.

Thus, **scheme** (5) becomes:

$$\begin{aligned} c_i^{n+1} = c_i^n + \frac{\Delta t}{\Delta x} \Bigg(& \frac{1}{2} v_{i+\frac{1}{2}} \left[(1+\beta_{i+\frac{1}{2}}) c_i^n + (1-\beta_{i+\frac{1}{2}}) c_{i+1}^n \right] + \\ & \frac{1}{4} |v_{i-\frac{1}{2}}| \left(1 - \left| \frac{v_{i-\frac{1}{2}} \Delta t}{\Delta x} \right| \right) \Delta x \left[(1+\beta_{i-\frac{1}{2}}) \sigma_{i-1}^n + (1-\beta_{i-\frac{1}{2}}) \sigma_i^n \right] - \\ & \frac{1}{2} v_{i+\frac{1}{2}} \left[(1+\beta_{i+\frac{1}{2}}) c_i^n + (1-\beta_{i+\frac{1}{2}}) c_{i+1}^n \right] - \\ & \frac{1}{4} |v_{i+\frac{1}{2}}| \left(1 - \left| \frac{v_{i+\frac{1}{2}} \Delta t}{\Delta x} \right| \right) \Delta x \left[(1+\beta_{i+\frac{1}{2}}) \sigma_i^n + (1-\beta_{i+\frac{1}{2}}) \sigma_{i+1}^n \right] \Bigg). \end{aligned} \tag{8}$$

The previous scheme (8) is known to be conservative but not necessarily monotonous [14, 9]. This non-monotonicity may produce numerical solutions with unrealistic oscillations. These oscillations are due to the high variation of the concentration slopes σ_i^n near jumps of the concentration. A way to measure these oscillations is to use the concept of Total Variation (TV) defined as

$$TV(\{c_i^n\}_{i=1}^I) = \sum_{i=1}^{I} |c_i^n - c_{i-1}^n|.$$

We are interested in creating numerical schemes with the property of Total Variation Diminution (TVD), that is $TV(\{c_i^n\}_{i=1}^I) \geq TV(\{c_i^{n+1}\}_{i=1}^I)$. That property ensures that the scheme will not develop oscillations. Thus, we now introduce a variation of the scheme (8) that guarantee TVD.

To do so, we introduce the concept of flux limiters. In (6), we replace $\Delta x \left[(1+\beta_{i-\frac{1}{2}})\sigma_{i-1}^n + (1-\beta_{i-\frac{1}{2}})\sigma_i^n\right]$ by $\phi(r_{i-\frac{1}{2}}^n)(c_i^n - c_{i-1}^n)$, and we obtain

$$\begin{aligned} f_{i-\frac{1}{2}}^{n-\frac{1}{2}} &= \frac{1}{2} v_{i-\frac{1}{2}} \left[(1+\beta_{i-\frac{1}{2}})c_{i-1}^n + (1-\beta_{i-\frac{1}{2}})c_i^n\right] + \\ &\quad \frac{1}{4}|v_{i-\frac{1}{2}}| \left(1 - \left|\frac{v_{i-\frac{1}{2}}\Delta t}{\Delta x}\right|\right) \phi(r_{i-\frac{1}{2}}^n)(c_i^n - c_{i-1}^n), \end{aligned} \tag{9}$$

where $\phi(r)$ is called flux limiter and $r_{i-\frac{1}{2}}^n = \dfrac{c_{i-1}^n - c_{i-2}^n}{c_i^n - c_{i-1}^n}$ if $v_{i-\frac{1}{2}} \geq 0$ or $= \dfrac{c_{i+1}^n - c_i^n}{c_i^n - c_{i-1}^n}$ if $v_{i-\frac{1}{2}} < 0$. On a similar way we can rewrite

$$\begin{aligned} f_{i+\frac{1}{2}}^{n+\frac{1}{2}} &= \frac{1}{2} v_{i+\frac{1}{2}} \left[(1+\beta_{i+\frac{1}{2}})c_i^n + (1-\beta_{i+\frac{1}{2}})c_{i+1}^n\right] + \\ &\quad \frac{1}{4}|v_{i+\frac{1}{2}}| \left(1 - \left|\frac{v_{i+\frac{1}{2}}\Delta t}{\Delta x}\right|\right) \phi(r_{i+\frac{1}{2}}^n)(c_{i+1}^n - c_i^n), \end{aligned} \tag{10}$$

where $r_{i-\frac{1}{2}}^n = \dfrac{c_i^n - c_{i-1}^n}{c_{i+1}^n - c_i^n}$ if $v_{i+\frac{1}{2}} \geq 0$ or $= \dfrac{c_{i+2}^n - c_{i+1}^n}{c_{i+1}^n - c_i^n}$ if $v_{i+\frac{1}{2}} < 0$.

Then, scheme (8) can be rewritten as

$$\begin{aligned} c_i^{n+1} &= c_i^n + \frac{\Delta t}{\Delta x}\Bigg(\frac{1}{2} v_{i+\frac{1}{2}} \left[(1+\beta_{i+\frac{1}{2}})c_i^n + (1-\beta_{i+\frac{1}{2}})c_{i+1}^n\right] + \\ &\quad \frac{1}{4}|v_{i-\frac{1}{2}}| \left(1 - \left|\frac{v_{i-\frac{1}{2}}\Delta t}{\Delta x}\right|\right) \phi(r_{i-\frac{1}{2}}^n)(c_i^n - c_{i-1}^n) - \\ &\quad \frac{1}{2} v_{i+\frac{1}{2}} \left[(1+\beta_{i+\frac{1}{2}})c_i^n + (1-\beta_{i+\frac{1}{2}})c_{i+1}^n\right] - \\ &\quad \frac{1}{4}|v_{i+\frac{1}{2}}| \left(1 - \left|\frac{v_{i+\frac{1}{2}}\Delta t}{\Delta x}\right|\right) \phi(r_{i+\frac{1}{2}}^n)(c_{i+1}^n - c_i^n)\Bigg). \end{aligned} \tag{11}$$

We note that if in scheme (11) we take:

- $\phi(r) = 0$, we recover the first order upwind scheme (a scheme producing a high level of artificial diffusion).
- $\phi(r) = \dfrac{1}{2}(1+r)$, we recover the Fromm scheme.
- $\phi(r) = 1$, we recover the Lax-Wendroff scheme.
- $\phi(r) = r$, we recover the Beam-Warming scheme.

The first scheme is first order accurate and TVD. The second, third and fourth schemes are second order accurate, but non-TVD.

Let us consider the following nonlinear flux limiters:

- $\phi(r) =$minmod$(1, r)$, we obtain the minmod scheme [25].
- $\phi(r) = \max(0, \min(1, 2r), \min(2, r))$, we obtain the superbee scheme [25].
- $\phi(r) = \max(0, \min((1+r)/2, 2, r))$, we recover the monotonized central scheme [31].
- $\phi(r) = (r + |r|)/(1 + |r|)$, we recover the Van Leer scheme [30].
- $\phi(r) = (r^2 + r)/(r^2 + 1)$, we recover the Van Albada 1 scheme [29].

The five above schemes are TVD.

In the following sub-section we are going to introduce a two-dimensional version of scheme (11).

3.2 Approximation of problems (1) and (2)

The Finite Volume method is well-suited to the space-time discretization of problem (1). Namely, the positive integers I and J being given, we divide the spatial domain $\Omega_{i,j} = (x_{1,\min}, x_{1,\max}) \times (x_{2,\min}, x_{2,\max})$ into IJ control volumes $\Omega_{i,j}$. More precisely, for $i = 1, \ldots, I$, $j = 1, \ldots, J$, we define $\Omega_{i,j}$ by

$$\begin{aligned} \Omega_{i,j} = (x_{1,\min} + (i-1)\Delta x_1, x_{1,\min} + i\Delta x_1) \\ \times (x_{2,\min} + (j-1)\Delta x_2, x_{2,\min} + j\Delta x_2), \end{aligned} \tag{12}$$

with $\Delta x_1 = \dfrac{x_{1,\max} - x_{1,\min}}{I}$, $\Delta x_2 = \dfrac{x_{2,\max} - x_{2,\min}}{J}$.

For simplicity, we will present only a fully explicit scheme, of the forward Euler type, for the time discretization of problem (1); constructing implicit or semi-implicit variants of the scheme to be described below is pretty easy.

Let Δt^n be the time step at the n-th step of the scheme; Δt^n is defined by

$$\Delta t^n = \min(\Delta t^n_{\mathrm{CFL}}, \Delta t_{\mathrm{pump}}),$$

where $\Delta t^n_{\mathrm{CFL}}$ denotes the Courant-Friedrichs-Lewy (CFL) upper bound that Δt^n has to verify at the n-th step, for the scheme to be stable; $\Delta t^n_{\mathrm{CFL}}$ is given by

$$\Delta t^n_{\mathrm{CFL}} = \frac{\mathcal{C}\Delta x_1 \Delta x_2}{\Delta x_1 \overline{V}^n_1 + \Delta x_2 \overline{V}^n_2},$$

where $\mathcal{C} \in [0,1]$ is the CFL constant ($\mathcal{C} = 1$, typically, for explicit schemes, to ensure that the flow is no further than one grid element, at most, during the time step [7]); the quantities $\overline{V}_1^n = \max_{(i=1,\ldots,I+1;j=1,\ldots,J)} V^n_{1,i-\frac{1}{2},j}$ and $\overline{V}_2^n = \max_{(i=1,\ldots,I;j=1,\ldots,J+1)} V^n_{2,i,j-\frac{1}{2}}$ are defined below. Furthermore, Δt_{pump} denotes the maximum time step that can be considered for the 'reaction' term so that during the time step one grid element cannot be emptying more than its contaminant quantity; Δt_{pump} is given by

$$\Delta t_{\text{pump}} = \frac{\Delta x_1 \Delta x_2}{2\pi Q}. \tag{13}$$

We note that for an implicit time discretization scheme, there is no limitation on the time step as long as stability is concerned; of course accuracy requires small time steps.

Let $C^0_{i,j} = c_0(\xi_{i,j})$ with $\xi_{i,j}$ being the center of cell $\Omega_{i,j}$. On each cell $\Omega_{i,j}$, for $i = 1,\ldots,I$ and $j = 1,\ldots,J$ at time step n we compute $C^{n+1}_{i,j} = C^{n+1}(\xi_{i,j})$ as follows.

For the diffusion term in (2), we consider the discretization scheme:

$$\begin{aligned}
\mathcal{D}(i,j,n) = \;& 2\Delta t^n \left(\frac{C^n_{i,j}}{c_{\text{ref}}}\right)^{\kappa} \left(\frac{d_1}{(\Delta x_1)^2} + \frac{d_2}{(\Delta x_2)^2}\right) C^n_{i,j} \\
& - \frac{d_1 \Delta t^n}{(\Delta x_1)^2} \left(\left(\frac{C^n_{i+1,j}}{c_{\text{ref}}}\right)^{\kappa} C^n_{i+1,j} + \left(\frac{C^n_{i-1,j}}{c_{\text{ref}}}\right)^{\kappa} C^n_{i-1,j} \right) \\
& - \frac{d_2 \Delta t^n}{(\Delta x_2)^2} \left(\left(\frac{C^n_{i,j+1}}{c_{\text{ref}}}\right)^{\kappa} C^n_{i,j+1} + \left(\frac{C^n_{i,j-1}}{c_{\text{ref}}}\right)^{\kappa} C^n_{i,j-1} \right)
\end{aligned} \tag{14}$$

For the transport term, we consider the scheme with limiters described below.

$$\begin{aligned}
\mathcal{A}^+_{\mathbf{V}}(1,i,j,n) = \;& \left[\sigma^+_{1,i,j,n} + \phi(q_{1,i,j,n})\vartheta(\sigma^+_{1,i,j,n})\right] C^n_{i,j} \\
& - \Big[\sigma^+_{1,i-1,j,n} + \big(\phi(q_{1,i,j,n})\vartheta(\sigma^+_{1,i,j,n}) \\
& + \phi(q_{1,i-1,j,n})\vartheta(\sigma^+_{1,i-1,j,n})\big)\Big] C^n_{i-1,j} \\
& + \left[\phi(q_{1,i-1,j,n})\vartheta(\sigma^+_{1,i-1,j,n})\right] C^n_{i-2,j},
\end{aligned}$$

and

$$\begin{aligned}\mathcal{A}^-_{\mathbf{V}}(1,i,j,n) = \quad & \big[\sigma^-_{1,i,j,n} + \phi(r_{1,i,j,n})\vartheta(\sigma^-_{1,i,j,n})\big]C^n_{i,j} \\ & -\big[\sigma^-_{1,i+1,j,n} + \big(\phi(r_{1,i,j,n})\vartheta(\sigma^-_{1,i,j,n}) \\ & +\phi(r_{1,i+1,j,n})\vartheta(\sigma^-_{1,i+1,j,n})\big)\big]C^n_{i+1,j} \\ & +\big[\phi(r_{1,i+1,j,n})\vartheta(\sigma^-_{1,i+1,j,n})\big]C^n_{i+2,j},\end{aligned}$$

and

$$\begin{aligned}\mathcal{A}^+_{\mathbf{V}}(2,i,j,n) = \quad & \big[\sigma^+_{2,i,j,n} + \phi(q_{2,i,j,n})\vartheta(\sigma^+_{2,i,j,n})\big]C^n_{i,j} \\ & -\big[\sigma^+_{2,i,j-1,n} + \big(\phi(q_{2,i,j,n})\vartheta(\sigma^+_{2,i,j,n}) \\ & +\phi(q_{2,i,j-1,n})\vartheta(\sigma^+_{2,i,j-1,n})\big)\big]C^n_{i,j-1} \\ & +\big[\phi(q_{2,i,j-1,n})\vartheta(\sigma^+_{2,i,j-1,n})\big]C^n_{i,j-2},\end{aligned}$$

and

$$\begin{aligned}\mathcal{A}^-_{\mathbf{V}}(2,i,j,n) = \quad & \big[\sigma^-_{2,i,j,n} + \phi(r_{2,i,j,n})\vartheta(\sigma^-_{2,i,j,n})\big]C^n_{i,j} \\ & -\big[\sigma^-_{2,i,j+1,n} + \big(\phi(r_{2,i,j,n})\vartheta(\sigma^-_{2,i,j,n}) \\ & +\phi(r_{2,i,j+1,n})\vartheta(\sigma^-_{2,i,j+1,n})\big)\big]C^n_{i,j+1} \\ & +\big[\phi(r_{2,i,j+1,n})\vartheta(\sigma^-_{2,i,j+1,n})\big]C^n_{i,j+2},\end{aligned}$$

where

- $\vartheta(a) = \dfrac{a}{2}(1-a)$;
- $\sigma^+_{1,i,j,n} = (\max(0, V^n_{1,i,j-\frac{1}{2}})\Delta t^n)/\Delta x_1$;
- $\sigma^-_{1,i,j,n} = (|\min(0, V^n_{1,i,j-\frac{1}{2}})|\Delta t^n)/\Delta x_1$;
- $\sigma^+_{2,i,j,n} = (\max(0, V^n_{2,i-\frac{1}{2},j})\Delta t^n)/\Delta x_2$;
- $\sigma^-_{2,i,j,n} = (|\min(0, V^n_{2,i-\frac{1}{2},j})|\Delta t^n)/\Delta x_2$;
- $q_{1,i,j,n} = \dfrac{C^n_{i+1,j} - C^n_{i,j}}{C^n_{i,j} - C^n_{i-1,j}}$;
- $q_{2,i,j,n} = \dfrac{C^n_{i,j+1} - C^n_{i,j}}{C^n_{i,j} - C^n_{i,j-1}}$;

- $r_{k,i,j,n} = \dfrac{1}{q_{k,i,j,n}}$, with k=1,2;
- $V^n_{1,i,j-\frac{1}{2}} = V_1((x_{1,\min} + i\Delta x_1, x_{2,\min} + (j - \dfrac{1}{2})\Delta x_2), \sum_{i=1}^n \Delta t^i)$;
- $V^n_{2,i-\frac{1}{2},j} = V_2((x_{1,\min} + (i - \dfrac{1}{2})\Delta x_1, x_{2,\min} + j\Delta x_2), \sum_{i=1}^n \Delta t^i)$.
- $\mathbf{V}(x,t) = (V_1(x,t), V_2(x,t)) = \mathbf{w}(x,t) + \mathbf{s}(x,t) + \mathbf{p}_{\text{tol}}(x,t)$, is the velocity field with $x \in \Omega$ and $t \in [0,T]$.

Then, we denote

$$\mathcal{A}_{\mathbf{V}}(i,j,n) = \mathcal{A}^+_{\mathbf{V}}(1,i,j,n) + \mathcal{A}^-_{\mathbf{V}}(1,i,j,n) + \mathcal{A}^+_{\mathbf{V}}(2,i,j,n) + \mathcal{A}^-_{\mathbf{V}}(2,i,j,n)$$

For the (kind of) reaction term associated with the pumping process, we have the following scheme:

$$\mathcal{R}(i,j,n) = \Delta t^n \frac{2\pi R_p Q}{\Delta x_1 \Delta x_2} C^n_{i_p,j_p} \chi^{p,n}_{i,j} \tag{15}$$

where $\Omega_{i_{p,n},j_{p,n}}$ is the cell containing $\gamma_p(n\Delta t)$ and $\chi^{p,n}_{i,j} = 0$ if $\{i,j\} \neq \{i_{p,n}, j_{p,n}\}$, $\chi^{p,n}_{i,j} = 1$ if $\{i,j\} = \{i_{p,n}, j_{p,n}\}$.

Thus, the complete discretized scheme proposed for system (1) is:

$$C^n_{i,j} = C^{n-1}_{i,j} - \mathcal{D}(i,j,n-1) - \mathcal{A}_{\mathbf{V}}(i,j,n-1) - \mathcal{R}(i,j,n-1). \tag{16}$$

This scheme is completed by the following discrete version of the boundary condition of system (2).

for $i = 1, ..., I$ and $j = 1, ..., J$, we have

$$\begin{aligned}
C^n_{I+1,j} &= \frac{\Delta t^n}{L}\Bigg[\bigg(\frac{L}{\Delta t^n} + \min(0, V^{n-1}_{1,I,j-\frac{1}{2}})\bigg)C^{n-1}_{I+1,j} \\
&\quad + \max(0, V^{n-1}_{1,I,j-\frac{1}{2}})C^{n-1}_{I,j} \\
&\quad - \Big(\frac{C^{n-1}_{I+1,j} + C^{n-1}_{I,j}}{2c_{\text{ref}}}\Big)^{\kappa}\frac{d_1}{\Delta x_1}\Big(C^{n-1}_{I+1,j} - C^{n-1}_{I,j}\Big)\Bigg], \\
C^n_{0,j} &= \frac{\Delta t^n}{L}\Bigg[\bigg(\frac{L}{\Delta t^n} + \max(0, V^{n-1}_{1,0,j-\frac{1}{2}})\bigg)C^{n-1}_{0,j} \\
&\quad + \min(0, V^{n-1}_{1,0,j-\frac{1}{2}})C^{n-1}_{1,j} \\
&\quad - \Big(\frac{C^{n-1}_{0,j} + C^{n-1}_{1,j}}{2c_{\text{ref}}}\Big)^{\kappa}\frac{d_1}{\Delta x_1}\Big(C^{n-1}_{1,j} - C^{n-1}_{0,j}\Big)\Bigg], \\
C^n_{i,J+1} &= \frac{\Delta t^n}{L}\Bigg[\bigg(\frac{L}{\Delta t^n} + \min(0, V^{n-1}_{2,i-\frac{1}{2},J})\bigg)C^{n-1}_{i,J+1} \\
&\quad + \max(0, V^{n-1}_{2,i-\frac{1}{2},J})C^{n-1}_{i,J} \\
&\quad - \Big(\frac{C^{n-1}_{i,J+1} + C^{n-1}_{i,J}}{2c_{\text{ref}}}\Big)^{\kappa}\frac{d_2}{\Delta x_2}\Big(C^{n-1}_{i,J+1} - C^{n-1}_{i,J}\Big)\Bigg], \\
C^n_{i,0} &= \frac{\Delta t^n}{L}\Bigg[\bigg(\frac{L}{\Delta t^n} + \max(0, V^{n-1}_{2,i-\frac{1}{2},0})\bigg)C^{n-1}_{i,0} \\
&\quad + \min(0, V^{n-1}_{2,i-\frac{1}{2},0})C^{n-1}_{i,1} \\
&\quad - \Big(\frac{C^{n-1}_{i,0} + C^{n-1}_{i,0}}{2c_{\text{ref}}}\Big)^{\kappa}\frac{d_2}{\Delta x_2}\Big(C^{n-1}_{i,1} - C^{n-1}_{i,0}\Big)\Bigg].
\end{aligned}$$

We note that if in scheme (16) we take

- $\phi(r) = 0$ we obtain the first order upwind scheme,
- $\phi(r) = \frac{1}{2}(1 + r)$ we obtain the Fromm scheme,
- $\phi(r) = 1$ we obtain the Lax-Wendroff scheme,
- $\phi(r) = r$ we obtain the Beam-Warming scheme,
- $\phi(r) =$minmod$(1, r)$ we obtain the minmod scheme,
- $\phi(r) = \max(0, \min(1, 2r), \min(2, r))$ we obtain the superbee scheme,

- $\phi(r) = \max(0, \min((1+r)/2, 2, r))$ we recover the monotonized central scheme,
- $\phi(r) = (r + |r|)/(1 + |r|)$ we recover the Van Leer scheme,
- $\phi(r) = (r^2 + r)/(r^2 + 1)$ we recover the Van Albada 1 scheme.

3.3 An alternative splitting scheme

If an explicit scheme is used to treat the advection part of the mathematical model given by (1), the numerical model discussed in Section 3.2 is computationally quite expensive. In order to reduce the computational time we propose to consider a splitting technique.

Basically, the velocity field can be divided in two main components:

- the first one is the sea and wind currents $\mathbf{w}(x,t) + \mathbf{s}(x,t)$,
- the second one is the advection generated by the pump $\mathbf{p}_{\text{tol}}(x,t)$.

As shown in the numerical experiments presented in the next section, the velocity $\mathbf{p}_{\text{tol}}$ is much higher than $\mathbf{w} + \mathbf{s}$ generating small time steps due to the CFL condition. However, the effect of the pumping process is quite limited in space.

Thus, in order to reduce the computational effort we propose to split our scheme in those two velocities components. More precisely, to compute the solution from time t^{n-1}up to time t^n we first consider the intermediate step that handle the evolution of the solution $C_{i,j}^{n-1}$ considering only the effect of the wind and sea currents and diffusion from time t^{n-1} up to t^n:

$$\tilde{C}_{i,j}^{n} = C_{i,j}^{n-1} - \mathcal{D}(i,j,n-1) - \mathcal{A}_{\mathbf{V}}(i,j,n-1), \tag{17}$$

with $\Delta t_{\text{CFL}}^n = \dfrac{\mathcal{C}\Delta x_1 \Delta x_2}{\Delta x_1 \overline{V}_1^n + \Delta x_2 \overline{V}_2^n}$ and $\mathbf{V} = \mathbf{w} + \mathbf{s}$.

Then, starting from the intermediate solution $\tilde{C}_{i,j}^{n}$, we compute the evolution of the general solution from time t^{n-1} up to t^n by considering only the effect of the pump.

To do so, we consider the smallest square domain, denoted by $\mathcal{S}(t)$, containing $B(\gamma(t), R_{\text{tol}})$, the ball of center $\gamma(t)$ and radius R_{tol} in which $\mathbf{p}_{\text{tol}} > 0$.

Next, we use the following scheme

$$\bar{C}_{i,j}^{n_p} = \bar{C}_{i,j}^{n_p-1} - \mathcal{A}_{\mathbf{p}_{\text{tol}}}(i,j,n_p-1) - \mathcal{R}(i,j,n_p-1), \text{in } \mathcal{S}^{n_p}, \tag{18}$$

where $n_p = 1, ..., n_p^{\max}$, $\bar{C}_{i,j}^0 = \tilde{C}_{i,j}^n$, $\mathcal{S}^{n_p} = \mathcal{S}(t^{n-1} + n_p \Delta t_{\mathrm{CFL}}^{p_{\mathrm{tol}}})$, $\mathbf{p}_{\mathrm{tol}} = (p_{\mathrm{tol},1}, p_{\mathrm{tol},2})$, $\Delta t_{\mathrm{CFL}}^{p_{\mathrm{tol}}} = \dfrac{\mathcal{C}\Delta x_1 \Delta x_2}{\Delta x_1 p_{tol,1} + \Delta x_2 p_{\mathrm{tol},2}}$, $n_p^{\max}$ =ceil$(\dfrac{t^n - t^{n-1}}{\Delta t_{\mathrm{CFL}}^{p_{\mathrm{tol}}}})$, ceil$(\xi)$ rounds ξ upwards to the nearest integer.

Finally,

$$C_{i,j}^n = C_{i,j}^{n_p^{\max}}.$$

4 Numerical Experiments

4.1 Synopsis

In this section, we will check the efficiency of the computational methods discussed in Section 3. It will be done by performing a variety of numerical experiments, all related to real life situations. Also the results obtained from models (1) and (2) will be compared.

Remark 1 *Anticipating on the results to be presented in Section 4.2, we would like to note that in order to obtain numerical results as accurate as possible, only fully explicit schemes are considered there, avoiding thus those additional errors produced by the solution of the linear systems associated with implicit schemes. Moreover, after performing various additional experiments (not presented here) relying on implicit or hybrid implicit-explicit schemes, we observed that the time steps Δt^n required to obtain an accuracy comparable to the accuracy of the explicit scheme were much smaller than $\Delta t_{\mathrm{CFL}}^n$ (from the explicit scheme CFL stability condition), another reason for favoring explicit schemes.*

4.2 The pollution scenario considered for the numerical simulations

We have considered numerical experiments and model parameters based on real data. More precisely, the initial shape and characteristics of the oil spill and the wind and sea currents are based on the Prestige hazard [19]. This event was caused by the sinking of an oil tanker in 2002 near the coast of the Spanish province of Galicia. Around 6.3×10^4 tons of oil were spilled on the open sea (at 200 km from the nearest coast).

The domain Ω is defined by $x_{1,\min} = 0$, $x_{1,\max} = 8 \times 10^4$ m, $x_{2,\min} = 0$ and $x_{2,\max} = 8 \times 10^4$ m. The characteristic length L occurring in the boundary conditions of model (2) is given by $L = 11.3 \times 10^4$ m.

The simulation time is equal to one day, $T = 86400$ s.

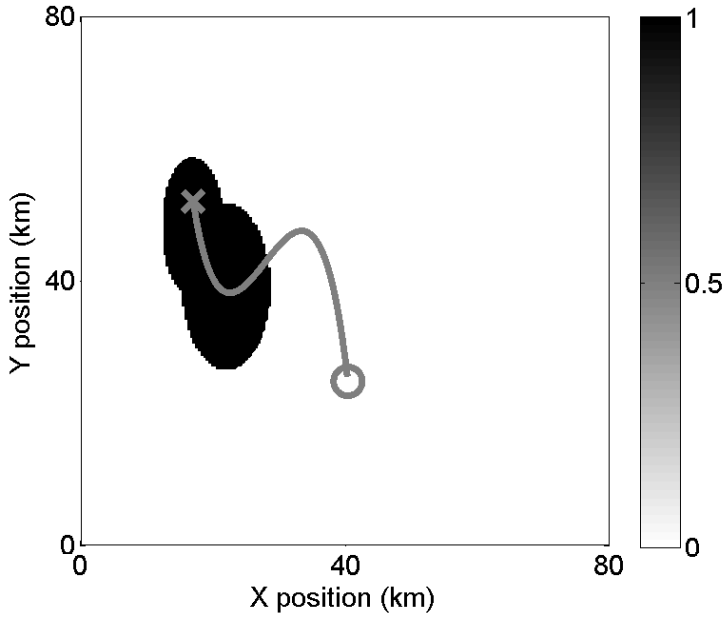

Figure 1: Position of the pollutant spot at time $t = 0$. The initial (**X**) and final (**o**) positions and the trajectory (−) of the skimmer ship are also shown (in gray).

The diffusion coefficient of the oil in sea water is set to $d_1 = d_2 = 0.5$ m s^{-1} [20]. The oil density is 870 kg m^{-3} [8] and its average thickness is 2 $\times 10^{-4}$ m [27]. The tolerance value is tol= 0.05 m s^{-1}. The initial position of the oil spill in Ω, presented in Figure 1, is given by

$$c(\xi, 0) = \chi_{E(17000,49000,4700,10000)}(\xi) + \chi_{E(22000,38000,7000,13000)}(\xi), \qquad (19)$$

where $\xi = (\xi_1, \xi_2) \in \Omega$ and $\chi_{E(a,b,c,d)}(\xi) = 1$ if $(\xi_1 - a)^2/c + (\xi_2 - b)^2/d \leq 1$ and 0 elsewhere.

The wind plus sea velocity field $\mathbf{V}(x,t) = (V_1(x,t), V_2(x,t)) = \mathbf{s}(x,t) + \mathbf{w}(x,t)$, expressed in m s^{-1}, is inspired from observations provided by [6, 1]. It is defined by

$$\begin{aligned} V_1(x,t) &= \frac{2}{9} - \frac{1}{9}\sin\left(\frac{\pi\Delta t}{172800}\right) + \frac{x_1}{540000} \\ V_2(x,t) &= \left(\frac{1}{5} - \frac{1}{10}\cos(\frac{\pi\Delta t}{172800})\right)\frac{2}{3}\sin\left(\pi(\frac{1}{2} + \frac{x_2}{60000})\right), \end{aligned} \qquad (20)$$

for $t \in [0, T]$ and $x = (x_1, x_2) \in \Omega$.

The skimmer ship characteristics are based on the A-Whale Super Tanker Vessel [4]. This ship was used during the BP Deepwater Horizon oil spill in the **Gulf of Mexico** hazard in 2010. The pump parameters are $Q = 6.5$ m s^{-1} and $R_p = 113$ m. The pumping ship follows the trajectory described in Figure 1 which is generated by cubic spline interpolation trough the points (17000,52000) a time $t = 0$ s, (23000,38000) at $t = 28200$ s, (33000,47500) at time $t = 56400$ s and (25000,41000) at $t = 84600$ s.

4.3 Linear vs Nonlinear Diffusion Models

Our goal in this section is to compare the results obtained from the *linear* diffusion model (1) and the *nonlinear* diffusion model (2).

To do so, we performed four numerical experiments. In each one we considered a spatial discretization mesh using $(I, J) = (100, 100)$. The time discretization scheme was explicit (to avoid -see Remark 1- the numerical errors produced by the solution of linear systems); the time step was set at $\Delta t = 864$ s (considered small enough to produce accurate results [2]).

In the first experiment, denoted by **Diff lin**, we solved numerically the linear diffusion problem

$$\begin{cases} \dfrac{\partial c}{\partial t} - \nabla \cdot \mathbf{d} \nabla c = 0, & \text{in } \Omega \times (0, T), \\ \dfrac{\partial c}{\partial t} + \dfrac{\mathbf{d} \partial c}{L \partial \mathbf{n}} = 0, & \text{on } \partial\Omega \times (0, T), \\ c = c_0, & \text{in } \Omega \times \{0\}, \end{cases} \tag{21}$$

with the parameters provided in Section 4.2.

In the second, third and fourth experiments, denoted by **Diff nl**κ with $\kappa = 1, 2$ and 3, we solved numerically the nonlinear diffusion problem

$$\begin{cases} \dfrac{\partial c}{\partial t} - \nabla \cdot \dfrac{c^\kappa}{c_{\text{ref}}^\kappa} \mathbf{d} \nabla c = 0, & \text{in } \Omega \times (0, T), \\ \dfrac{\partial c}{\partial t} + \dfrac{c^\kappa}{c_{\text{ref}}^\kappa} \dfrac{\mathbf{d} \partial c}{L \partial \mathbf{n}} = 0, & \text{on } \partial\Omega \times (0, T), \\ c = c_0, & \text{in } \Omega \times \{0\}, \end{cases} \tag{22}$$

with the parameters provided in Section 4.2 and $c_{\text{ref}} = 1$.

In each of these experiments, we are interested in computing

- **CPUT**: The CPU time needed to solve numerically the initial value problems (21) and (22).

- **LOSS**: The numerical mass loss in percentage of the oil concentration between the initial and final times. It is computed as:

$$100\left(\sum_{i,j=1}^{I,J} C_{i,j}^{N} \Big/ \sum_{i,j=1}^{I,J} C_{i,j}^{0}\right), \tag{23}$$

  where N is the value of n associated with the last time step of the numerical scheme (that is $N = \dfrac{T}{\Delta t}$). This quantity measures the conservation property of our numerical scheme.

- $\mathbf{NFV}_{\delta}$: The number of volume elements filled with an oil concentration greater than δ (a nonnegative real number suitably small). $\mathbf{NFV}_{\delta}$ is a measure of the effect on the polluted spots expansion due to the diffusion velocity and artificial diffusion of the schemes under consideration.

In Table 1, we present the results obtained when performing the experiments **Diff lin**, **Diff nl1**, **Diff nl2** and **Diff nl3**. Regarding the $\mathbf{NFV}_{\delta}$ values, choosing in this case $\delta = 0$, we see that the final concentration for the linear diffusion model reaches the boundary of the whole domain Ω. This is due to the infinite speed of propagation of linear diffusion. When using the nonlinear schemes this value is reduced by 90% compared to the linear one and do not reach this boundary. Furthermore, as expected, the larger is κ the lower is the expansion of the oil spots due to diffusion effects (velocity and artificial). This can be seen on Figure 2, where the final concentration distribution and zero-contours generated by the nonlinear diffusion models are depicted. As a consequence, the numerical mass loss values of the nonlinear schemes are null. Moreover, the CPU time resulting from the linear model is four times larger than the one taken by the nonlinear ones.

Those results show the efficiency of the nonlinear scheme in controlling the undesired effects of the linear diffusion. **The choice of κ is an important issue (and also a complicated one, since κ varies with the crude oil under consideration), however we failed at finding numerical values of this parameter in the open literature (it is likely that oil companies have quantitative information about κ, but they do not tell). From now on, we will use the nonlinear scheme with $\kappa = 1$.**

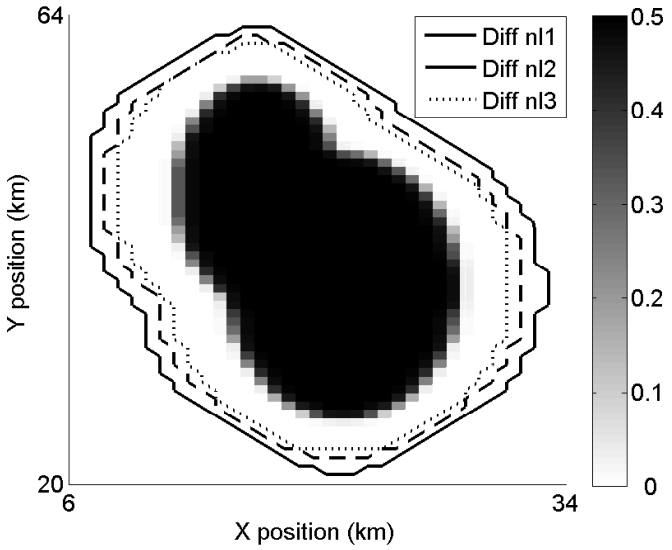

Figure 2: Distribution of the final oil concentration and zero-concentration contours, generated by the nonlinear diffusion models **Diff nl1**, **Diff nl2** and **Diff nl3**.

Experiment	CPUT	LOSS	$\mathbf{NFV}_0$
Diff lin	198	10^{-12}	10000
Diff nl1	53	0	1349
Diff nl2	51	0	1106
Diff nl3	50	0	1002

Table 1: Results obtained for the experiments presented in Section 4.3: **CPUT**, **LOSS** and $\mathbf{NFV}_0$ values of the different types of diffusion.

4.4 Comparison of different advection schemes

Now, we compare the performances of the different advection schemes presented in Section 3.1. We consider the advection equation:

$$\begin{cases} \dfrac{\partial c}{\partial t} + \nabla \cdot c\,(\mathbf{w} + \mathbf{s}) = 0, & \text{in } \Omega \times (0,T), \\ c = c_0, & \text{in } \Omega \times \{0\}, \end{cases} \tag{24}$$

with the parameters provided in Section 4.2. Here, we assume that the support of the initial condition is compact and strictly inside our domain of integration, and that the support of the solution at time t does not reach the boundary either.

We perform various numerical experiments corresponding to the following nine numerical schemes for the numerical solution of (24): **Adv DC** (Donor Cell), **Adv BW** (Beam and Warming), **Adv LW** (Lax-Wendroff), **Adv FR** (Fromm), **Adv MM** (Min-Mod), **Adv SB** (Super Bee), **Adv MC** (monotonized central), **Adv VL** (Van Leer) and **Adv VA** (Van Albada).

In all those experiments we consider $(I, J) = (100, 100)$ and an explicit time discretization scheme with $\Delta t = 864$ s (lower than the 1-CFL condition time step ≈ 2000 s). For each one, we compute the **CPUT**, **LOSS**, $\mathbf{NFV}_\delta$ values as defined in Section 4.2 and 4.3. In this case $\delta = 10^{-8}$, which is a value small enough to measure the artificial diffusion of the considered schemes. Moreover, we also check the apparition of negative values or concentration provoked by the non monotonicity of a scheme by defining **NVC**=0 if the concentration at each time step is non negative and 1 otherwise).

In Table 2, we show the obtained results. We observe that the CPU times are of the same order but the faster one is the Donor Cell linear scheme. However, the artificial diffusion of this scheme produces the higher $\mathbf{NFV}_{10^{-8}}$ value. This spot expansion measure is reduced when considering second order schemes. When regarding the linear second order schemes

(i.e., **BW**, **LW** and **FR**), we observe the occurrence of unwanted negative concentration values and a higher **LOSS** value due to the numerical oscillations generated by those schemes (i.e., non monotonicity). This can be also observed in Figure 3, where the final concentration distributions of the oil and their 10^{-8}-contours obtained by **Adv DC**, **Adv FR** and **Adv SB** (chosen as representative cases) are depicted. We observe that the shape of the spot generated with **Adv DC** is more diffuse than with second order schemes. However, regarding the contours, we observe the oscillations produced by the linear second order model **Adv FR**. The solution produced with the nonlinear second order model **Adv SB** clearly shows that this kind of scheme controls artificial diffusion and monotonicity. Thus, the nonlinear second order schemes should be preferred. Among them, the Super Bee (**SB**) exhibits the lowest spot expansion value and will be used for the next experiments presented here.

Experiment	**CPUT**	**NVC**	**LOSS**	$\mathbf{NFV}_{10^{-8}}$
Adv DC	442	1	10^{-14}	3275
Adv BW	543	0	10^{-10}	4392
Adv LW	482	0	10^{-10}	2826
Adv FR	504	0	10^{-10}	3321
Adv MM	542	1	10^{-14}	2345
Adv SB	631	1	10^{-14}	1416
Adv MC	636	1	10^{-14}	1457
Adv VL	489	1	10^{-14}	1637
Adv VA	484	1	10^{-14}	2198

Table 2: Results obtained for the experiments presented in Section 4.4: **CPUT**, **LOSS**, **NVC** and $\mathbf{NFV}_{10^{-8}}$ values of the different schemes for the advection.

4.5 Dirichlet vs absorbing boundary condition

In this section we discuss the advantage of using an absorbing boundary condition, instead of a Dirichlet one, to better simulate those cases where the oil spot crosses the boundary of the computational domain.

To do so, we introduce $\Omega_h = [0, 4\times10^4]\times[0, 8\times10^4]$ m, representing half of the domain Ω in the x_1-direction, and we solve the initial value problems (1) and (2) on Ω_h, without pumping (i.e. $Q = 0$), the other parameters being those provided in Section 4.2. The resulting solutions are denoted by

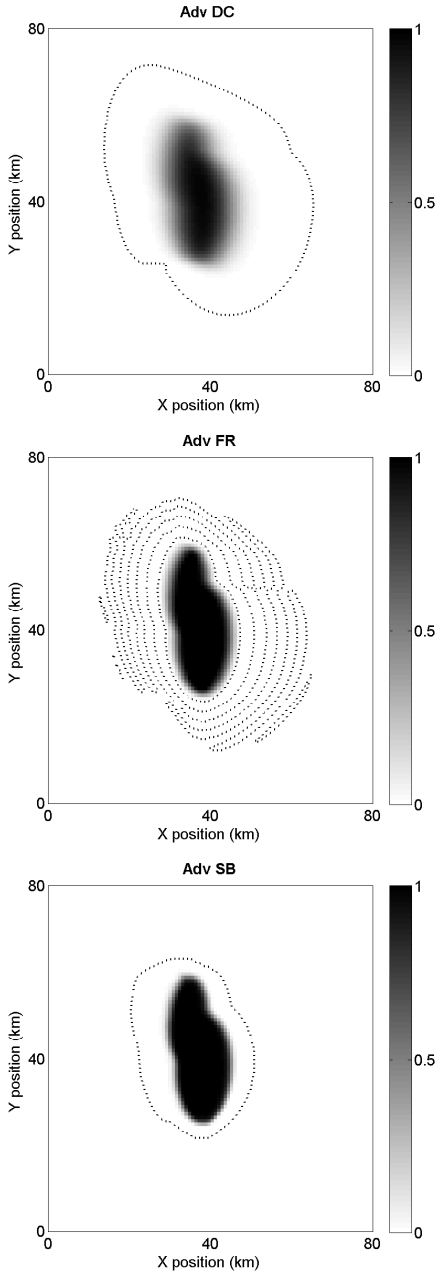

Figure 3: Distribution of the final oil concentration and 10^{-8}-concentration contours (dotted line), generated by the advection models **Adv DC** (Top-Left), **Adv FR** (Top-Right) and **Adv SB** (Bottom).

ADDH (Advection-Diffusion Dirichlet condition Half domain) and **ADAH** (Advection-Diffusion Absorbing condition Half domain), respectively. We observe that in these cases, the oil spot crosses the right boundary of Ω_h.

We compare previous solutions obtained on Ω_h with the solution of problem (2), computed in the whole domain Ω without pumping (i.e. $Q = 0$), the other parameters being like those provided in Section 4.2. The solution is denoted by **ADAF** (Advection-Diffusion Absorbing condition Full domain). Here, the oil spot does not reach the boundary of Ω; the related solution can be considered as a reference solution.

The three initial value problems associated with **ADDH**, **ADAH** and **ADAF** were solved taking (I, J)=(100,100), $\kappa = 1$ in the nonlinear diffusion term, and using the nonlinear Super Bee scheme to treat the advection; no splitting was employed. Once these simulations were performed, we computed the differences between these solutions near the right boundary of Ω_h; to be more precise, we computed

$$\mathbf{EAA} = \int_{38\text{km}}^{40\text{km}} \int_{0\text{km}}^{80\text{km}} |\mathbf{ADAF} - \mathbf{ADAH}| \mathrm{dx}_1 \mathrm{dx}_2 \tag{25}$$

and

$$\mathbf{EDI} = \int_{38\text{km}}^{40\text{km}} \int_{0\text{km}}^{80\text{km}} |\mathbf{ADAF} - \mathbf{ADDH}| \mathrm{dx}_1 \mathrm{dx}_2, \tag{26}$$

respectively.

We obtained **EAA**= 1.1×10^6 kg and **EDI**= 2.9×10^6 kg, implying that the difference associated with the absorbing boundary condition is-approximately-three times smaller than the one for the Dirichlet condition. This improvement appears clearly on Figure 4 where some contours of the **ADDH**, **ADAH** and **ADAF** solutions have been visualized; we observe that the **ADAH** contours fit better the **ADAF** contours than the **ADDH** ones.

From these results it appears that the absorbing boundary condition that we use produces a better approximation of the physical solution close to the boundary of the computational domain, than the Dirichlet's one.

4.6 Splitting vs. un-split schemes

Finally, we want to verify if it is advantageous to use splitting schemes. In order to achieve that goal, we performed the following numerical experiments, taking into account the results presented in Sections 4.3-4.4:

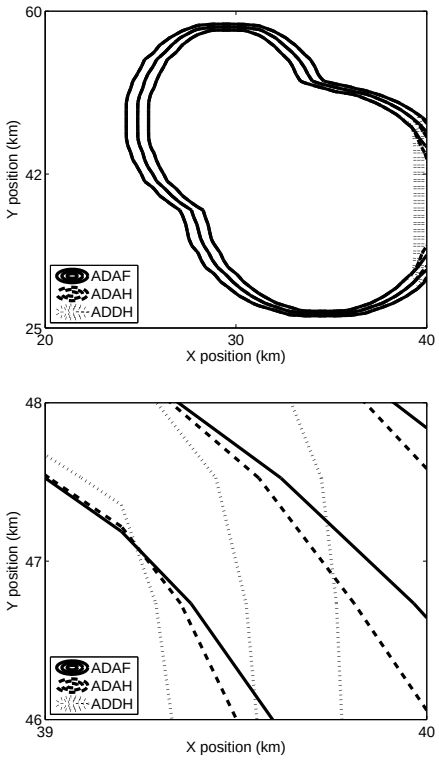

Figure 4: Some contours of the oil concentration distribution generated by the **ADAF** (—), **ADAH** (- -) and **ADDH** (...) numerical models introduced in Section 4.5. **Left**: Domain $(2 \times 10^4, 4 \times 10^4) \times (2.5 \times 10^4, 6 \times 10^4)$ m. **Right**: Near boundary domain $(3.9 \times 10^4, 4 \times 10^4) \times (4.6 \times 10^4, 4.8 \times 10^4)$ m.

- **ADR DC**: Solution of problem (1), using the linear first order Donor-Cell scheme to treat the advection, no splitting being used.
- **ADR SB**: Solution of problem (2) with $\kappa = 1$ in the nonlinear diffusion term, using the nonlinear second order Super Bee scheme to treat the advection, no splitting being used.
- **ADR SB-S**: Solution of problem (2) with $\kappa = 1$ in the nonlinear diffusion term, using the nonlinear second order Super Bee scheme to treat the advection. This time, the operator-splitting method described in Section 3.3 was used.

These numerical experiments were performed using four different meshes, namely (I, J)=(50, 50), (100,100), (150,150) and (200,200), the associated 1-CFL condition giving 500s, 125s, 56s and 31s, respectively, for the maximal value of Δt^n.

For each experiment, we computed the values of **CPUT** and $\mathbf{NFV}_{10^{-8}}$ (both defined in Section 4.4). Actually, we also computed:

- **PPUM**: The percentage of pumped oil at the end of the simulation with respect to its initial quantity.
- **LOCV**: The percentage of remaining oil at the end of the simulation with respect to its initial quantity plus the **PPUM** value. It measures the conservation property of our numerical models.

Results are presented in Table 3. They show the same behavior for the four grids we considered. The $\mathbf{NFV}_{10^{-8}}$ values of the **ADR SB** and **ADR SB-S** models are of the same order and between twice and three times smaller than **ADR DC**. In addition, employing splitting allows us to drastically reduce the CPU time in comparison to the other two models. Also, the **LOCV** values of **ADR SB** and **ADR SB-S** are lower than the **ADR DC** ones. Thus, **ADR SB-S** provides serious improvements with respect to **ADR SB**. This can also be noted on Figure 5, where the final pollutant concentration and the 10^{-8}-contour obtained by those three models are presented. Models **ADR SB** and **ADR SB-S** clearly exhibit similar behavior whereas the linear model **ADR DC** is more diffusive.

5 Conclusions

In this article we have presented an improved version of the model discussed in [2, 12], for simulating the evolution of oil spots in the open sea, taking into

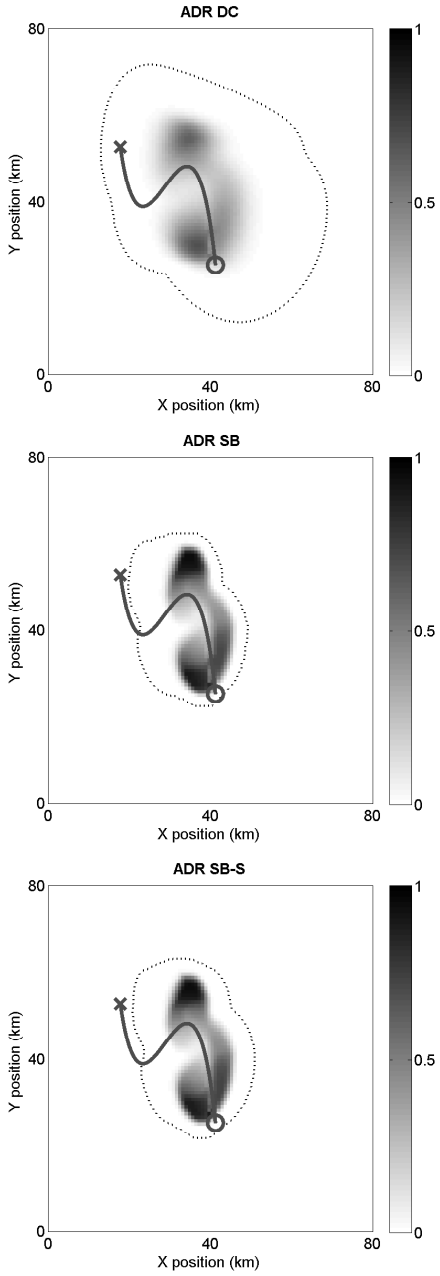

Figure 5: Distribution of the final oil concentration and 10^{-8}-concentration contours (..), generated by the advection models **ADR DC** (Top-Left), **ADR SB** (Top-Right) and **ADR SB-S** (Bottom). The initial position (**X**), the final position (**o**) and trajectory (–) of the pump are also shown.

Experiment	$I = J$	**PPUM**	**CPUT**	**LOCV**	$\mathbf{NFV}_{10^{-8}}$
ADR DC	50	45	183	10^{-7}	1387
ADR SB	50	51	238	10^{-13}	510
ADR SB-S	50	50	62	10^{-13}	528
ADR DC	100	47	4179	10^{-12}	3675
ADR SB	100	50	5450	10^{-13}	1310
ADR SB-S	100	49	427	10^{-13}	1395
ADR DC	150	47	31961	10^{-14}	6664
ADR SB	150	49	43361	10^{-14}	2392
ADR SB-S	150	49	1720	10^{-14}	2549
ADR DC	200	48	144365	10^{-14}	10254
ADR SB	200	49	176028	10^{-14}	3764
ADR SB-S	200	49	4312	10^{-14}	4004

Table 3: Results from the experiments described in Section 4.6: Values of **PPUM**, **CPUT**, **LOCV** and $\mathbf{NFV}_{10^{-8}}$ for the three models and four meshes which have been considered.

account: wind, sea currents and the effect of a skimmer ship used for the oil cleaning by pumping. Our objectives were to better control the artificial diffusivity, the velocity of the diffusion propagation, and the behavior of the computed solution at the boundary of the computational domain.

To achieve the goals listed above, we have: (i) Introduced a nonlinear diffusion term leading to diffusion effects propagating at finite velocity. (ii) Used second order accurate time discretization schemes with nonlinear limiters to treat the advection; these schemes have little artificial diffusion and good monotonicity conservation properties. (iii) Used an absorbing boundary condition to improve (with respect to the Dirichlet boundary condition) the behavior of the computed solutions near the boundary of the computational domain, particularly when the drifting oil spot crosses this boundary. (iv) Finally, to reduce the computational time required by our simulations, we used an operator-splitting method.

To verify the efficiency of the approach based on model (2), by comparison to the initial approach, based on model (1), and thoroughly discussed in [2] and [12], we have performed a large variety of numerical experiments, using parameters borrowed from real data of the 2002 Prestige hazard (which took place on the Spanish coast).

First, we observed that the nonlinear diffusion model, we use in the

present article, leads to a diffusion propagating at finite velocity, unlike the diffusion associated with (1), moreover the computational time is smaller.

Secondly, we compared various linear and nonlinear second order accurate finite difference schemes to treat the advection terms in (2). The best results were obtained using a second order scheme based on the Super-Bee nonlinear limiter, a scheme producing very little artificial diffusion, when applied to the solution of (2).

Finally, the introduction in (2) of boundary conditions, with good absorbing properties, on the boundary of the computational domain, produce a simulation method which creates little disturbance when the oil spot comes near the above boundary, and even crosses it: a behavior very different from the one which is observed if one prescribes a homogeneous Dirichlet condition at the boundary of the computational domain.

Acknowledgments

This work was carried out thanks to the financial support of the Spanish "Ministry of Economy and Competitiveness" under project MTM2011-22658; the research group MOMAT (Ref. 910480) supported by "Banco Santander" and "Universidad Complutense de Madrid"; the "Junta de Andalucía" and the European Regional Development Fund through project P12-TIC301; and the PAPIIT project of the National University of Mexico. The authors would like to thank Nelson del Castillo for his valuable help during this work.

This document is a preprint of an article submitted for consideration in Mathematical Models and Methods in Applied Sciences ©. February 3, 2015. Copyright World Scientific Publishing Company. URL:
`http://www.worldscientific.com/worldscinet/m3as`

References

[1] A.J. Abascal, S. Castanedo, F.J. Mendez, R. Medina, and I.J. Losada, Calibration of a Lagrangian Transport Model Using Drifting Buoys Deployed during the Prestige Oil Spill, Journal of Coastal Research, 251 (2009), 80–90.

[2] C. Alavani, R. Glowinski, S. Gomez, B. Ivorra, P. Joshi, A.M. Ramos, Modelling and simulation of a polluted water pumping process, Mathematical and Computer Modelling, 51 (2010), 461–472.

[3] X. Antoine, A. Arnold, C. Besse, M. Ehrhardt, A. Schädle, A Review of Transparent and Artificial Boundary Conditions Techniques for . Linear and Nonlinear Schrödinger Equations. Communications In Computational Physics, 4(4) (2008), 729–796.

[4] Auke Visser. Historical Tankers Site. A-Whale characteristics. Available at: http://www.aukevisser.nl/supertankers/bulkers/id453.htm

[5] A.D. Carpenter, R.G. Dragnich, Marine Operations and Logistics During the Exxon Valdez Spill Cleanup, Oil Spill Conference Proceedings 1991, pp. 205-211, 1991.

[6] S. Castanedo, R. Medina, I.J. Losada, C. Vidal, F.J. Mndez, J. Osorio, A. Puente, The Prestige oil spill in Cantabria (Bay of Biscay). Part I: Operational forecasting system for quick response, risk assessment and protection of natural resources, Journal Of Coastal Research, 22(6) (2006), 1474–1489.

[7] R. Courant, K. Friedrichs, H. Lewy, On the partial difference equations of mathematical physics, IBM Journal of Research and Development 11 (2) (1967), 215–234.

[8] P.S. Daling, M.O. Moldestad, The Prestige Oil-Weathering Properties. Marine Environmental Technology. 2 (2003), 1–4.

[9] C.P. Dullemond. Lecture on: Numerical Fluid Dynamics. University of Heidelberg, Summer Semester, 2008. Website: http://www.mpia.de /homes/dullemon/lectures/fluiddynamics08/

[10] B. Engquist, A. Majda, Absorbing boundary conditions for the numerical simulation of waves, Math. Comp., 31 (1977), 629-651.

[11] R. Glowinski, P. Neittaanmaki, Partial Differential Equations. Modelling and Numerical Simulation, Series: Computational Methods in Applied Sciences, Springer,16, 2008.

[12] S. Gomez, B. Ivorra, A.M. Ramos, Optimization of a pumping ship trajectory to clean oil contamination in the open sea, Mathematical and Computer Modelling, 54(1) (2011), 477-489.

[13] K. Gustafson, Domain Decomposition, Operator Trigonometry, Robin Condition, Contemporary Mathematics, 218 (1998), 432-437.

[14] C. Hirsch, Numerical Computation of Internal and External Flows: The Fundamentals of Computational Fluid Dynamics (Second Edition), Butterworth-Heinemann Ltd, 2007.

[15] W. Hundsdorfer, J.G. Verwer, Numerical Solution of Time-Dependent Advection-Diffusion-Reaction Equations, Springer Series in Comput. Math. 33, 2003.

[16] D. Kr oner, Absorbing boundary conditions for the linearized Euler equations in 2-d, Mathematics of Computation, 57(195) (1991), 153–167.

[17] J.L. Lions, E. Magenes, Problemes aux limites non homogenes et applications - Volume 2, Dunod, 1968.

[18] Merv Fingas. The Basics of Oil Spill Cleanup, Second Edition, CRC Press, 2000.

[19] P. Montero, J. Blanco, J.M. Cabanas, J. Maneiro, Y. Pazos, A. Moroo, C.F. Balseiro, P. Carracedo, B. Gmez, E. Penabad, V. Perez-Muuzuri, F. Braunschweig, R. Fernades, P.C. Leitao and R. Neves. Oil Spill Monitoring, Forecasting on the Prestige-Nassau accident. In: Proceedings 26th Arctic Marine Oil Spill Program (AMOP) Technical Seminar, 2 (2003), 1013–1029.

[20] S.P. Murray, Turbulent Diffusion of Oil in the Ocean, J. Limnology and Oceanography, 17(5) (1972): 651–660.

[21] Nihoul, J.C.J. Hydrodynamical and biochemical state variables and evolution equations for the mathematical modelling of sea pollution. in: Nihoul, J.C.J. (Ed.) Third Lige Colloquium on Ocean Hydrodynamics, University of Lige. Mmoires de la Socit Royale des Sciences de Lige. Sixime Srie, 2 (1972), 111–123

[22] N.O.A.A., Oil Spill case histories 1967-1991. Summaries of significant U.S. and international spills, Office of response and restoration of the U.S. National Ocean, Report HMRAD 92-11, 1992.

[23] Office of response and restoration of the U.S. National Ocean Service, Website: http://response.restoration.noaa.gov

[24] Office of response and restoration of the U.S. National Ocean Service, Incident News Home, Website: http://incidentnews.gov

[25] P.L. Roe, "Characteristic-based schemes for the Euler equations, Ann. Rev. Fluid Mech. 18 (1986), 337–365.

[26] S.K. Skinner, W.K. Reilly, The Exxon Valdez Oil Spill. National Response Team, 2008.

[27] G. Tchobanoglous, F.L. Burton, H.D. Stensel, Wastewater Engineering, Treatment and Reuse. 4th ed, Metcalf and Eddy, New York: McGraw-Hill, 2003.

[28] United States Environmental Protection Agency, Oil Spill Response Techniques, Website: http://www.epa.gov/osweroe1/content/ learning/oiltech.htm, 2009.

[29] G.D. Van Albada, B. Van Leer, W.W. Roberts , A comparative study of computational methods in cosmic gas dynamics, Astron. Astrophysics 108 (1982), 76–84

[30] B. Van Leer, "Towards the ultimate conservative difference scheme II. Monotonicity and conservation combined in a second order scheme", J. Comp. Phys. 14 (4) (1974), 361–370.

[31] B. Van Leer, Towards the ultimate conservative difference scheme III. Upstream-centered finite-difference schemes for ideal compressible flow, J. Comp. Phys. 23 (3) (1977), 263–275.

[32] B. Van Leer, Towards the ultimate conservative difference scheme. IV. A new approach to numerical convection, J. Comput. Phys., 23 (3) (1977), 276–299.

[33] E.K. Wilson, Oil Spill's Size Swells, Chemical and Engineering News, American Chemical Society, 2010.